

Hyperparameter optimization and force error correction of neuroevolution potential for predicting thermal conductivity of wurtzite GaN

Zhuo Chen(陈卓), Yuejin Yuan(袁越锦), Wenyang Ding(丁文扬), Shouhang Li(李寿航), Meng An(安盟), and Gang Zhang(张刚)

Citation: Chin. Phys. B, 2025, 34 (**8**): 086110. DOI: 10.1088/1674-1056/add905
http://cpb.iphy.ac.cn; http://iopscience.iop.org/cpb

What follows is a list of articles you may be interested in

General-purpose moment tensor potential for Ga-In liquid alloys towards large-scale molecular dynamics with *ab initio* accuracy

Kai-Jie Zhao(赵凯杰) and Zhi-Gong Song(宋智功)
Chin. Phys. B, 2025, 34 (**6**): 066101. DOI: 10.1088/1674-1056/adc661

Effect of copper/tungsten heterophase interface on radiation resistance: Insights from atomistic simulations

Wen Chen(陈文), Min Li(李敏), Bao-Qin Fu(付宝勤), Tun Chen(陈暾), Jie-Chao Cui(崔节超), and Qing Hou(侯氢)
Chin. Phys. B, 2025, 34 (**4**): 046108. DOI: 10.1088/1674-1056/adb40d

Molecular dynamics simulations of collision cascades in polycrystalline tungsten

Lixia Liu(刘丽霞), Mingxuan Jiang(蒋明璇), Ning Gao(高宁), Yangchun Chen(陈阳春), Wangyu Hu(胡望宇), and Hiuqiu Deng(邓辉球)
Chin. Phys. B, 2025, 34 (**4**): 046103. DOI: 10.1088/1674-1056/adb410

Properties of radiation defects and threshold energy of displacement in zirconium hydride obtained by new deep-learning potential

Xi Wang(王玺), Meng Tang(唐孟), Ming-Xuan Jiang(蒋明璇), Yang-Chun Chen(陈阳春), Zhi-Xiao Liu(刘智骁), and Hui-Qiu Deng(邓辉球)
Chin. Phys. B, 2024, 33 (**7**): 076103. DOI: 10.1088/1674-1056/ad362b

Geometries and electronic structures of Zr_nCu(n =2-12) clusters: A joint machine-learning potential density functional theory investigation

Yizhi Wang(王一志), Xiuhua Cui(崔秀花), Jing Liu(刘静), Qun Jing(井群), Haiming Duan(段海明), and Haibin Cao(曹海宾)
Chin. Phys. B, 2024, 33 (**1**): 016109. DOI: 10.1088/1674-1056/acd5c2

SPECIAL TOPIC — Artificial intelligence and smart materials innovation: From fundamentals to applications

Hyperparameter optimization and force error correction of neuroevolution potential for predicting thermal conductivity of wurtzite GaN

Zhuo Chen(陈卓)[1,2], Yuejin Yuan(袁越锦)[1], Wenyang Ding(丁文扬)[3], Shouhang Li(李寿航)[4], Meng An(安盟)[3,†], and Gang Zhang(张刚)[2,‡]

[1] *College of Mechanical and Electrical Engineering, Shaanxi University of Science and Technology, Xi'an* 710049, *China*
[2] *Yangtze Delta Region, Academy of Beijing Institute of Technology, Jiaxing* 314019, *China*
[3] *Department of Mechanical Engineering, The University of Tokyo*, 7-3-1 *Hongo, Bunkyo, Tokyo* 113-8656, *Japan*
[4] *Centre de Nanosciences et de Nanotechnologies, CNRS, Université Paris-Saclay*, 10 *Boulevard Thomas Gobert*, 91120 *Palaiseau, France*

(Received 4 March 2025; revised manuscript received 5 May 2025; accepted manuscript online 15 May 2025)

As a representative of wide-bandgap semiconductors, wurtzite gallium nitride (GaN) has been widely utilized in high-power devices due to its high breakdown voltage and low specific on-resistance. Accurate prediction of wurtzite GaN's thermal conductivity is a prerequisite for designing effective thermal management systems for electronic applications. Machine learning-driven molecular dynamics simulation offers a promising approach to predicting the thermal conductivity of large-scale systems without requiring predefined parameters. However, these methods often underestimate the thermal conductivity of materials with inherently high thermal conductivity due to the large predicted force error compared with first-principles calculations, posing a critical challenge for their broader application. In this study, we successfully developed a neuroevolution potential for wurtzite GaN and accurately predicted its thermal conductivity, 259±6 W/(m·K) at room temperature, achieving excellent agreement with reported experimental measurements. The hyperparameters of the neuroevolution potential (NEP) were optimized based on a systematic analysis of reproduced energy and force, structural features, and computational efficiency. Furthermore, a force error correction method was implemented, effectively reducing the error caused by the additional force noise in the Langevin thermostat by extrapolating to the zero-force error limit. This study provides valuable insights and holds significant implications for advancing efficient thermal management technologies in wide-bandgap semiconductor devices.

Keywords: machine learning potential, molecular dynamics, thermal conductivity, gallium nitride

PACS: 61.82.Fk, 31.15.–p, 52.65.Yy, 74.25.fc

DOI: 10.1088/1674-1056/add905 **CSTR:** 32038.14.CPB.add905

1. Introduction

The wide-bandgap semiconductors, exemplified by GaN and SiC, have been widely utilized in high-power devices due to their high breakdown voltage and low specific on-resistance.[1] However, these high-power devices often operate under extreme conditions, such as high temperatures, high voltages, and high-frequency environments.[2] These conditions typically result in extremely high heat flux densities, which can adversely impact the stability and operational lifespan of devices.[3,4] Accurate prediction and characterization of the thermal conductivity of wurtzite GaN are essential for understanding its thermal transport mechanisms and designing efficient thermal management systems.

Over the past decades, extensive studies have focused on the prediction and characterization of the thermal conductivity of wurtzite GaN using both theoretical methods[5–7] and experimental measurements.[8–10] The measured thermal conductivity of wurtzite GaN has typically lacked a consistent conclusion, generally ranging from 180 W/(m·K) to 220 W/(m·K). This variability arises from differences in experimental samples, measurement methods, and the limited availability of single-crystalline wurtzite GaN samples. Recently, the development of high-purity wurtzite GaN samples has enabled the measurement of thermal conductivity up to 246 W/(m·K) through systematic experimental characterization.[11] However, first-principles calculation-based Boltzmann transport equations tend to overestimate the thermal conductivity of wurtzite GaN using the local-density approximation (LDA) form of the exchange–correlation function, primarily due to inconsistent lattice parameters with experimental samples and simplified anharmonicity calculations.[5,12] In contrast, our previous work[13] determined the thermal conductivity of wurtzite GaN to be 264 W/(m·K), employing the PBE form of the exchange-correlation function while maintaining consistent lattice parameters ($a = 3.184$ Å and $c = 5.187$ Å). This result aligns well with experimental measurements.[11]

†Corresponding author. E-mail: anmeng@sust.edu.cn
‡Corresponding author. E-mail: gangzhang2006@gmail.com

© 2025 Chinese Physical Society and IOP Publishing Ltd. All rights, including for text and data mining, AI training, and similar technologies, are reserved.

Similarly, molecular dynamics (MD) simulations using empirical potentials predicted a thermal conductivity of approximately 180 W/(m·K),[14,15] which is significantly lower than the reported experimental value.[11] Machine learning-driven molecular dynamics simulation offers a promising alternative for predicting the thermal conductivity of large-scale systems without the need for predefined parameters. However, these methods often underestimate the thermal conductivity of materials with inherently high thermal conductivity,[16,17] such as wurtzite GaN, posing a critical challenge for their broader applications.

In this work, we first developed the neuroevolution potential (NEP) for wurtzite GaN, a representative machine learning potential (MLP), where the NEP model effectively balances the trade-off between computational efficiency and accuracy compared with other machine learning potential models.[18,19] We systematically investigated the influence of NEP hyperparameters on the accuracy of thermal conductivity prediction and computational efficiency. Furthermore, we implemented a correction method to eliminate force prediction errors in the Langevin thermostat,[20] achieving an accurate thermal conductivity of 259±6 W/(m·K) at room temperature, which aligns closely with the experimental value.[11]

2. Methods

2.1. Neuroevolution potential training

In the NEP model, the radial and angular components are influenced by the cutoff radii r_c^R and r_c^A, respectively. In our study, three cutoff radii values (4.5 Å, 5.0 Å, and 5.5 Å) were evaluated to optimize the accuracy of the NEP model. We performed tests to determine the optimal cutoff values; other hyperparameters used to train the NEP model are listed in Table S1. In total, we gathered 404 structures for the training set and 180 structures for the testing set. The training set includes a unit cell, a supercell, 200 MD structures at temperatures ranging from 100 K to 1900 K, and 202 structures with small random atomic displacements and variations in lattice constants. We employed a general-purpose machine learning model, MACE-MP,[21] in conjunction with the atomic simulation environment (ASE) package,[22] to perform MD simulations using the canonical (NVT) ensemble. The testing set was generated by performing MD simulations involving heating from 100 K to 1900 K using the NEP model trained on the training set. Static calculations based on first-principles methods were performed to obtain the energy, atomic forces, and virials of each structure.

2.2. DFT calculations for reference data generation

First-principles calculations were performed using density functional theory (DFT) as implemented in the Vienna *ab initio* simulation package (VASP).[23] The unit cell of wurtzite GaN, as shown in Figs. 1(a)–1(c), belongs to a hexagonal system with the $P6_3mc$ space group. The converged lattice constants of wurtzite GaN were found to be $a = b = 3.219$ Å and $c = 5.243$ Å, which are approximately 1% larger than the experimental values ($a = 3.19$ Å and $c = 5.189$ Å). This discrepancy is attributed to the use of the PBE functional,[24] which tends to overestimate lattice constants. In order to eliminate artificial factors, the original lattice constants were not adjusted in this work. The hexagonal system was converted to a cubic lattice (Fig. 1(d)) with dimensions 9.65 Å×11.153 Å×10.487 Å for MD simulations used to build the datasets. Structural visualization was carried out using the VESTA package.[25]

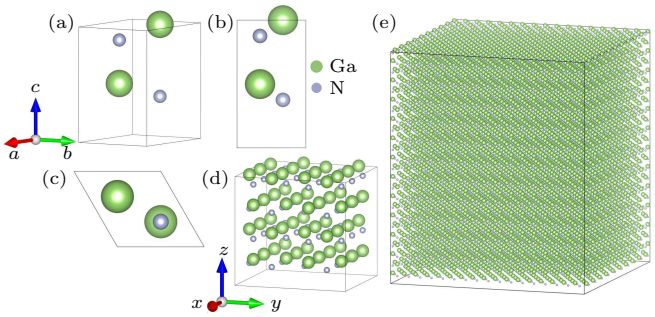


Fig. 1. Snapshots of (a)–(c) the unit cell of wurtzite GaN, (d) the supercell used in MACE-MP-based MD simulations, and (e) the supercell used for thermal conductivity calculations.

2.3. MD simulations

All MD simulations for thermal conductivity calculations were performed at 300 K using the GPUMD package[19] (version 3.9.4) with the NEP models (version 4).[26] The simulation process involved three distinct runs, each with a time step of 1 fs. The first run, lasting 0.5 ns, employed a stochastic cell rescaling (SCR) thermostat[27] within the isothermal-isobaric (NPT) ensemble, with a target pressure of zero. The second run, conducted for 0.2 ns, used a Bussi–Donadio–Parrinello (BDP) thermostat[28] in the NVT ensemble. Finally, a 15 ns simulation was performed in the NVT ensemble, during which the running thermal conductivity was recorded. We only considered the thermal conductivity of wurtzite GaN along the z-direction. The thermal conductivity was calculated using the homogeneous non-equilibrium molecular dynamics (HNEMD) method,[29] which is unique to GPUMD. Compared with the EMD method, the HNEMD method is more computationally efficient.[29] This performance difference stems from their fundamental methodological distinctions: EMD relies on measuring the heat current autocorrelation function (HCACF), whereas HNEMD directly evaluates the heat current. In EMD simulations, the noise-to-signal ratio in the decaying HCACF progressively increases with correlation time, leading to substantial fluctuations in the integrated running thermal conductivity, particularly at long correlation times, where only the averaged thermal conductivity

converges. Conversely, HNEMD simulations exhibit a constant noise-to-signal ratio in the measured heat current (as it does not decay over time), enabling rapid convergence of the running average. In this method, the heat current is proportional to the magnitude of the driving force parameter F_e, so careful selection of F_e is essential to ensure a large signal-to-noise ratio within the linear-response regime of the system.

To determine the parameter, we conducted extensive tests; the results are presented in Fig. 2(a). The system deviates from the linear-response regime when $F_e \geq 5\times10^{-5}$ Å^{-1}, while a small value of $F_e = 2\times10^{-6}$ Å^{-1} induces large fluctuations in thermal conductivity. Based on these observations, a value of $F_e = 2.5\times10^{-5}$ Å^{-1} was selected. Additionally, a sufficiently large simulation cell was used to eliminate finite-size effects. As shown in Fig. 2(b), we only considered the thermal conductivity of wurtzite GaN in the z-direction in this work, using a simulation cell with dimensions $L_x \times L_y \times L_z = 55.88$ Å$\times$54.83 Å$\times$63.08 Å (depicted in Fig. 1(e)), which contains 16320 atoms. MD simulations in classical statistical mechanics inherently adhere to the energy equipartition theorem. This framework leads to excessive excitation of high-frequency phonons, particularly below the Debye temperature, where quantum effects dominate. Such overpopulation of high-frequency phonons may induce significant overestimation of lattice thermal conductivity. In quantum statistical mechanics, only the vibrational modes with frequencies below the cutoff $k_BT \leq \hbar\omega_0$, where ω_0 is the vibrational frequency, contribute to the heat capacity, as described by Bose–Einstein statistics. To investigate the quantum effect, we employed a feasible quantum correction method based on spectral thermal conductivity, which is available within the HNEMD formalism. The spectral thermal conductivity is calculated as[30]

$$\kappa(\omega,T) = \frac{2C(\omega)}{VTF_e}, \tag{1}$$

where V is the volume, T is the temperature, and $C(\omega)$ is the virial-velocity correlation function in the frequency domain. $\kappa(\omega,T)$ can be quantum-corrected by multiplying it with the ratio between quantum and classical modal heat capacity[30–33]

$$\kappa^q(\omega,T) = \kappa(\omega,T)\frac{x^2e^x}{(e^x-1)^2}, \tag{2}$$

$$\kappa^q(T) = \int_0^\infty \frac{d\omega}{2\pi}\kappa^q(\omega,T), \tag{3}$$

where $x = \hbar\omega/k_BT$, $\hbar$ is the reduced Planck constant, and k_B is the Boltzmann constant. The total quantum-corrected thermal conductivity $\kappa^q(T)$ is obtained by integrating $\kappa^q(\omega,T)$ over the vibrational frequency.

The quantum-corrected spectral thermal conductivity at 300 K is presented in Fig. 2(c). We found that the thermal conductivity decreased by only 5% after quantum correction. This minimal change is attributed to the fact that the thermal conductivity of wurtzite GaN is primarily governed by low-frequency ($<$ 10 THz) phonons, which exhibit weak quantum effects. As a result, quantum corrections are not considered in the subsequent calculations.

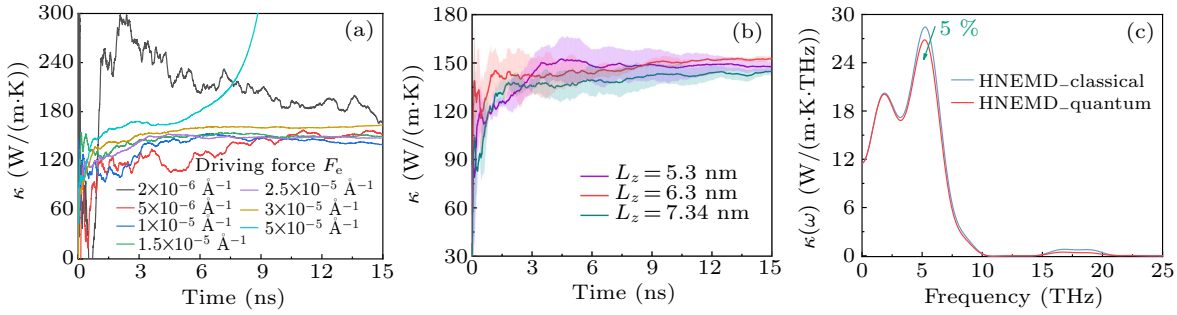


Fig. 2. (a) Cumulative average of the thermal conductivity of wurtzite GaN at 300 K and zero pressure. The driving force parameter F_e (listed in the legend) ranges from 2×10^{-6} Å^{-1} to 5×10^{-3} Å^{-1}. (b) Cumulative average of the thermal conductivity of wurtzite GaN at 300 K and zero pressure. The length in the z-direction increases from 5.3 nm to 7.34 nm, with three independent runs performed. (c) Classical and quantum-corrected spectral thermal conductivity of wurtzite GaN at 300 K. The green arrow and number indicate the region where classical MD overestimates the thermal conductivity.

3. Results and discussion

3.1. Hyperparameter optimization of neuroevolution potential

The NEP model is an MLP, based on the feedforward neural network and employed to describe the interatomic interactions. In a neural network potential, increasing the number of neurons generally improves the accuracy until convergence. Therefore, the hyperparameters, such as the number of radial and angular descriptor components that are related to the number of neurons, often follow standard values. In MD simulations, when calculating short-range interactions, it is typically sufficient to account only for the contributions of particles within a cutoff distance. The introduction of truncation approximation greatly reduces the computational cost of interatomic interactions. However, the relationship between the accuracy and truncation of MLP is not monotonic, and there is usually an optimal cutoff that achieves the optimized training accuracy. Our calculations found that the NEP with the highest

accuracy was associated with a significantly slower computational speed. Therefore, we question whether a greater cutoff radius is necessary to achieve higher accuracy. In a previous study, the cutoff value was determined only after the accuracy test had been conducted.[34] In this work, we hope to do more comprehensive testing to determine a more reasonable cutoff value, which is very meaningful for the training process of standardizing NEP.

Figure 3 presents the training results of three NEP models with different cutoffs, including the radial (r_c^R) and angular (r_c^A) cutoffs. The diagonal plots show the errors between the energy and force predicted by the NEP models and those obtained from DFT calculations. Each point in the plots represents the energy and force predicted by NEP versus the corresponding DFT value. The diagonal lines are included to help identify any significant deviation, allowing for a visual assessment of prediction accuracy. As depicted in Figs. 3(a), 3(d), and 3(g), the loss curve plateaus as the number of training steps increases. The diagonal plots show the errors between the energy and force predicted by the NEP models and DFT calculations. The RMSEs for energy in the training set reveal a decreasing trend as the cutoff radius increases: 0.55 meV/atom for $r_c^R = r_c^A = 4.5$ Å, 0.46 meV/atom for $r_c^R = r_c^A = 5.0$ Å, and 0.40 meV/atom for $r_c^R = r_c^A = 5.5$ Å. Similarly, the force RMSEs demonstrate a consistent improvement with increasing cutoff radii, decreasing from 47.93 meV/Å for $r_c^R = r_c^A = 4.5$ Å, 40.77 meV/Å for $r_c^R = r_c^A = 5.0$ Å, and 34.47 meV/Å for $r_c^R = r_c^A = 5.5$ Å. These results indicate that enlarging the cutoff radius significantly enhances the accuracy of the NEP model for capturing both energy and force of DFT calculation due to better representation of longer-range atomic interactions. Upon the optimization of energy and force in NEP, we then evaluated the predictive structure information of wurtzite GaN using the NEPs. All atomic structures were relaxed for 0.5 ns at 300 K using a SCR thermostat in the NPT ensemble, followed by 0.2 ns at 300 K using a BDP thermostat in the NVT ensemble. The radial distribution function (RDF) $g(r)$ and the structural factor (SF) $S(r)$ are shown in Fig. 4(a). SF highlights the long-range order characteristic of crystalline materials. Interestingly, the structural features remain consistent across different cutoff radii, indicating that a cutoff radius of 4.5 Å or larger is sufficient to accurately capture and construct the crystalline structure of wurtzite GaN.

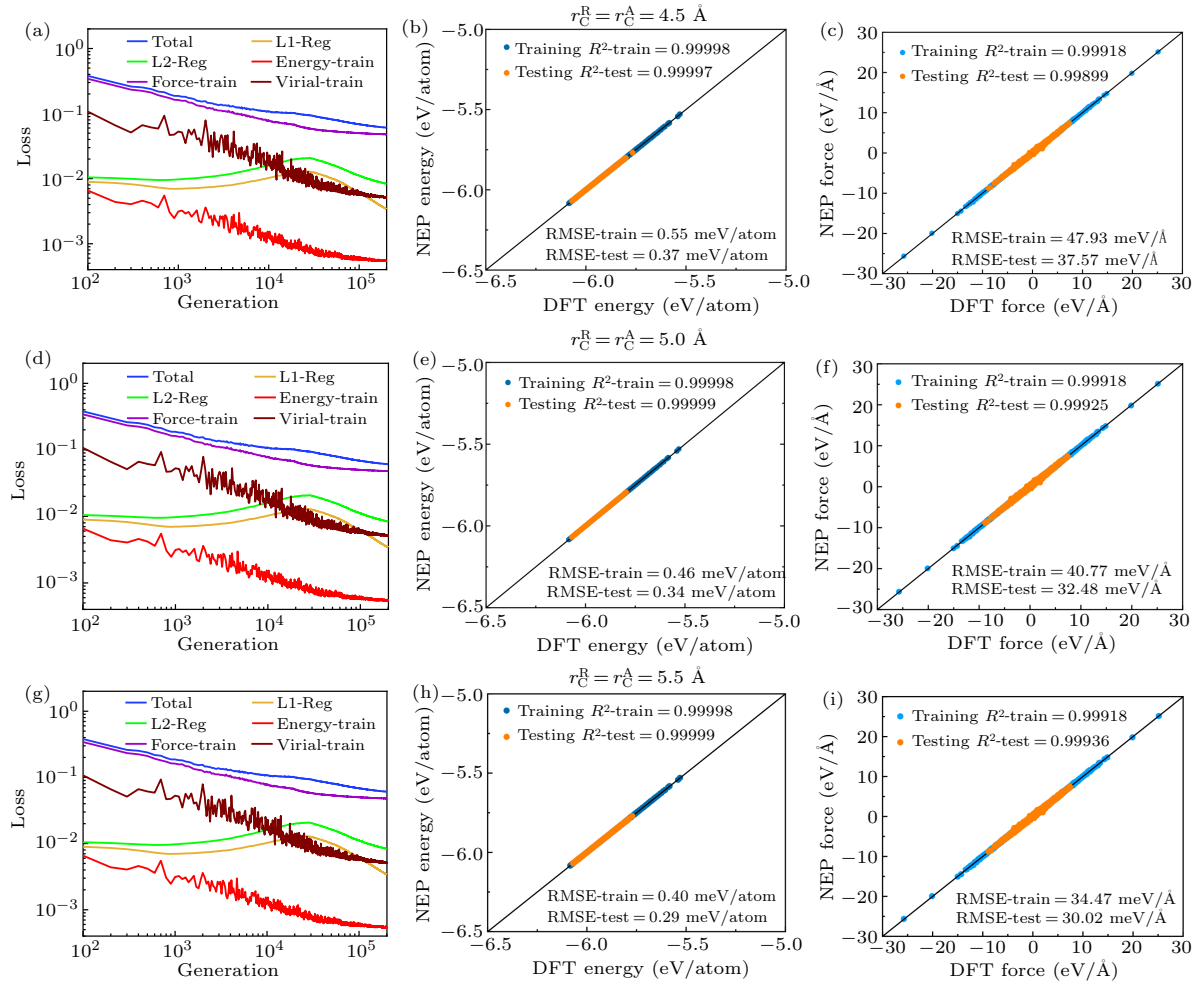


Fig. 3. Evolution of various terms in the loss function, including L1 and L2 regularization, energy RMSE (eV/atom), force RMSE (eV/Å), and virial RMSE (eV/atom) as a function of training generation for (a) 4.5 Å, (d) 5.0 Å, and (g) 5.5 Å. Energy from the NEP model compared with DFT reference data for (b) 4.5 Å, (e) 5.0 Å, and (h) 5.5 Å. Force from the NEP model compared with DFT reference data for (c) 4.5 Å, (f) 5.0 Å, and (i) 5.5 Å. The overall converged training and testing RMSEs and R^2 of energy and force are presented. Integrated cutoff values are indicated above each panel.

In addition to evaluating the structural features using the NEP models, the computational efficiency and accuracy in predicting the thermal conductivity of wurtzite GaN are equally critical. The thermal conductivity of wurtzite GaN along the z-direction was calculated using NEPs with varied cutoff radii, as shown in Fig. 4(b). Notably, the thermal conductivity of wurtzite GaN remains consistent, with differences of less than 2 W/(m·K) across the three cutoff radii. In contrast, the computational speed with a cutoff radius of 4.5 Å reaches approximately 9.8×10^6 atom-steps per second on a single Tesla A800 GPU, which is 78.2% faster compared to that with a cutoff radius of 5.5 Å. This significant improvement in computational efficiency highlights the advantage of adopting a smaller cutoff radius, which substantially reduces computational cost and time while maintaining accuracy in structural and thermal conductivity predictions.

Furthermore, the spectral thermal conductivity obtained with varying cutoff radii shows consistent results across the entire range of phonon frequencies, as illustrated in Fig. 4(c). Based on the above systematic analysis of the reproduced energy and forces, structural features, thermal conductivity predictions, computational efficiency, and spectral thermal conductivity from NEPs with varying cutoff radii, a cutoff radius of 4.5 Å was selected for subsequent thermal conductivity calculations, ensuring a balance between computational efficiency and accuracy.

To better demonstrate the phonon transport properties of wurtzite GaN, the phonon dispersions predicted by NEP and DFT are shown in Fig. 4(d). For the DFT calculations, there are four atoms in the primitive cell of GaN. The NEP model uses a supercell with 1024 atoms. Correspondingly, there are twelve phonon branches. The phonon frequencies predicted by NEP agree well with the DFT results and experimental data.[35]

Our work developed a NEP model and standardized the hyperparameter optimization process, which effectively addresses the trade-off between computational efficiency and predictive accuracy for thermal conductivity (Fig. 4). However, in previous studies,[30,36,37] the thermal conductivity was predicted using MLPs, with a primary focus on optimizing the hyperparameters to improve predictive accuracy.

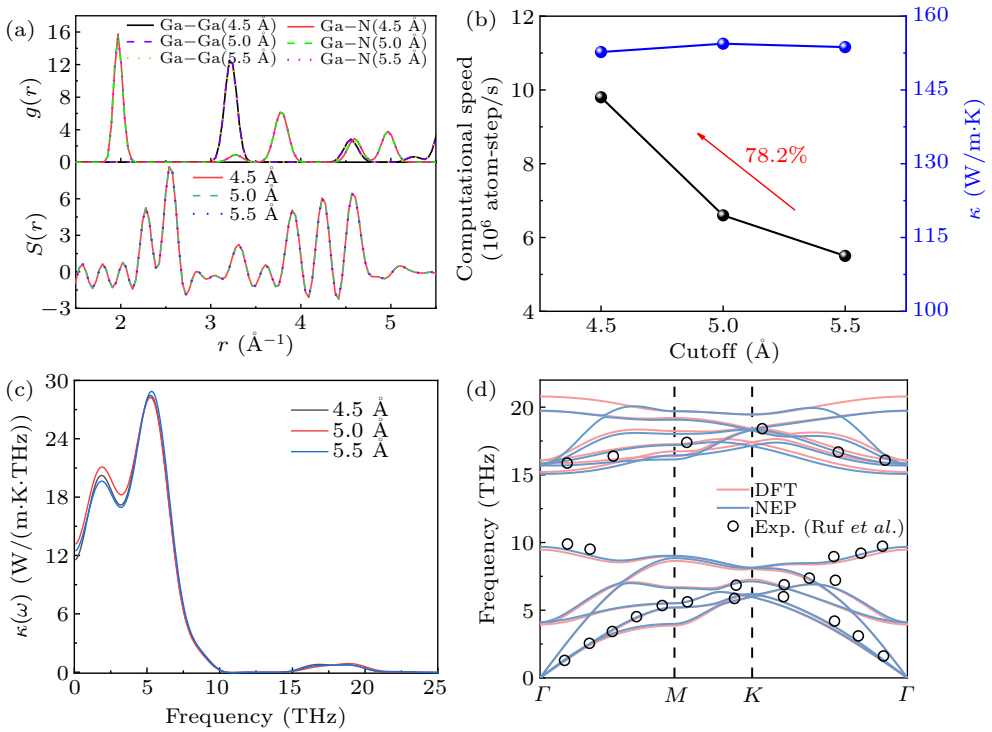


Fig. 4. (a) Radial distribution function $g(r)$ of Ga–Ga and Ga–N predicted by NEPs with various cutoff radii and the structure factors $S(r)$ of wurtzite GaN. (b) The computational speed (black axis) and thermal conductivities (blue axis) of wurtzite GaN predicted by NEPs with various cutoff radii. (c) The spectral thermal conductivities predicted by NEPs with various cutoff radii. (d) Phonon dispersions of GaN. Experimental data (symbols) are taken from Ruf *et al.*[35]

3.2. Correction of wurtzite GaN thermal conductivity

Despite extensive hyperparameter optimization of the NEP models, the calculated thermal conductivity of wurtzite GaN at 300 K was approximately 150 W/(m·K), which is significantly lower than the experimentally measured value of 246 W/(m·K)[11] and the DFT-predicted value of 260 W/(m·K).[7,38] This underestimation primarily arises from additional perturbations introduced by MLPs in molecular dynamics (MD) simulations, which enhance phonon–phonon scattering and consequently reduce thermal conductivity.[39,40]

Furthermore, our simulations were based on a perfect crystalline lattice of wurtzite GaN, whereas experimental sam-

ples often contain structural defects, which also act as phonon-scattering centers and can affect the observed thermal conductivity. Previous studies[16,17] have reported that MLPs generally tend to underestimate thermal conductivity, particularly in materials with intrinsically high thermal conductivities.

In MLP-based thermal conductivity calculations, residual force errors can arise due to discrepancies between the forces predicted by MLPs and the reference DFT-calculated forces. These discrepancies introduce additional noise into the energy and force landscape, which alters the heat flux distribution in MD simulations, effectively acting as a source of phonon-scattering. Studies[39,40] have shown that such residual force errors approximately follow a Gaussian distribution, analogous to stochastic forces (white noise) in the Langevin thermostat. This analogy permits the intentional introduction of tunable force noise via the Langevin thermostat to study its effect on phonon transport.

By systematically varying the magnitude of the applied noise, one can evaluate the thermal conductivity at different noise levels and extrapolate the results to estimate the intrinsic lattice thermal conductivity in the absence of force errors. To address this limitation, correction methods have been proposed to reconcile the discrepancy between MLP-predicted and experimentally measured thermal conductivities.[39,40] In this study, we adopted such a correction method to achieve a more accurate prediction of the thermal conductivity of GaN.

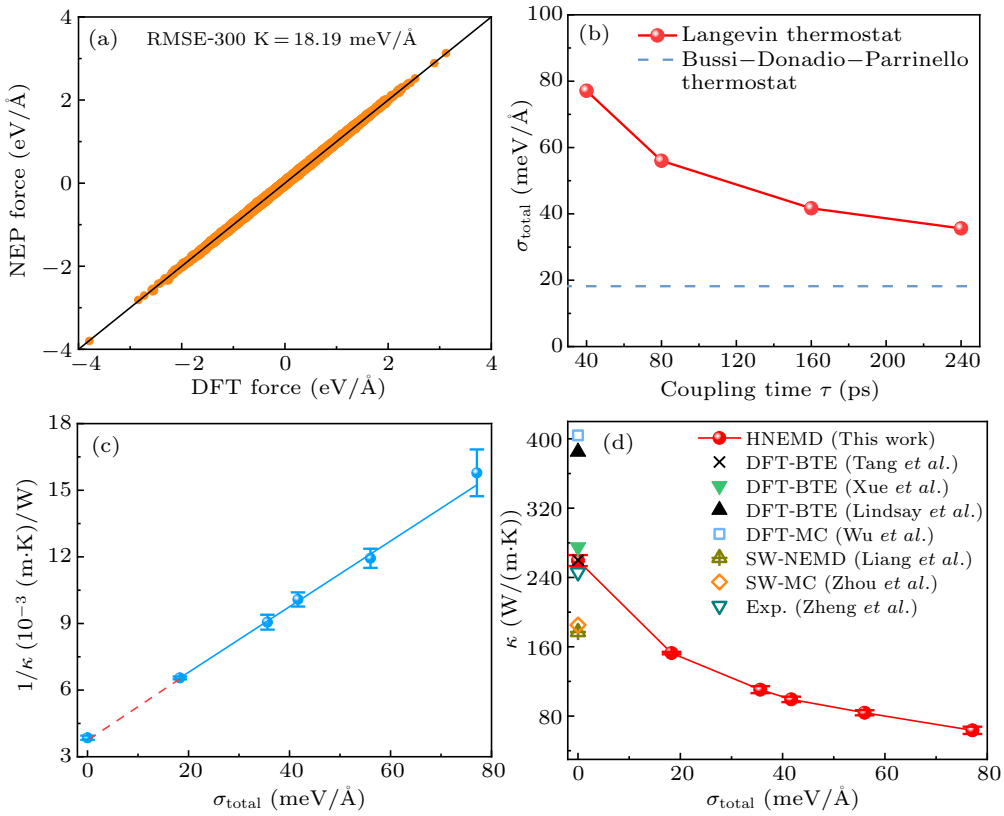


Fig. 5. (a) Force prediction of wurtzite GaN at 300 K from the NEP model compared with the DFT reference data. (b) Dependence of total force error σ_{total} on the coupling time. Red dots represent σ_{total} using the Langevin thermostat while the blue dotted line represents σ_{total} from the BDP thermostat, which remains unaffected by the coupling time. (c) Inverse thermal conductivity $(1/\kappa)$ from NEP-MD simulations as a function of σ_{total}. The solid line represents linear fits, and the red dotted line is an extrapolation of the results. The intersection points at $\sigma_{total} = 0$ correspond to the corrected thermal conductivity. (d) Calculated thermal conductivity as a function of σ_{total}. For comparison, DFT values,[5,7,12,38] SW results,[14,15] and experimental data[11] of thermal conductivity of wurtzite GaN at 300 K are also shown.

The core of the correction method lies in accounting for an additional force error, which follows a Gaussian distribution in the Langevin thermostat. This approach is analogous to the prediction error of forces observed in the NEP models, providing a systematic way to address discrepancies and enhance the accuracy of thermal conductivity prediction based on MLPs. This is because the Langevin thermostat does not directly regulate the dynamic state of the entire system, as a global thermostat such as the BDP thermostat does. Instead, it introduces random white noise forces to influence the dynamics of the system, resulting in an additional force error compared to a global thermostat. The magnitude of force error through the Langevin thermostat can be adjusted via the coupling time[39]

$$\sigma_{\mathrm{L}}^2 = \frac{2k_{\mathrm{B}}Tm_{\mathrm{ave}}}{\tau\Delta t}, \tag{4}$$

where m_{ave} is the average atomic mass, k_{B} is the Boltzmann constant, T is the temperature in the system, τ is the coupling time, and Δt is the time step. The total force error σ_{total} can be denoted as $\sigma_{\mathrm{total}} = \sqrt{\sigma_{\mathrm{nep}}^2 + \sigma_{\mathrm{L}}^2}$, where σ_{nep} is the RMSE of force prediction for the NEP model at the target temperature. The predicted thermal conductivity is inversely proportional to

σ_{total}, decreasing as σ_{total} increases. Based on a first-order approximation and Matthiessen's rule, the corrected thermal conductivity κ can be calculated using the following formula:[39]

$$\kappa_0 = \frac{1}{1/\kappa + \lambda\sigma_{\text{total}}}. \tag{5}$$

where κ is the wurtzite GaN thermal conductivity calculated by NEP-HNEMD with the Langevin thermostat, and λ is a fitting parameter.

We first evaluated the force prediction error of NEP in the MD-simulated structures at 300 K by comparing it to DFT reference data. These atomic configuration structures were generated through NEP-MD simulations using an SCR thermostat at 300 K, with 50 configurations uniformly sampled from a 1 ns trajectory for DFT static calculations. Figure 5(a) shows the σ_{nep} at 300 K, which can be considered as $\sigma_{\text{total}} = \sigma_{\text{nep}} = 18.19$ meV/Å when using the BDP thermostat. Notably, the force prediction error of the NEP model at 300 K in Fig. 5(a) is significantly lower than the overall force prediction error in Fig. 3(c). This is because the training set also includes high-temperature and perturbed structures, which are typically more force-intensive and require the model to predict the temperature-specific error accurately. Subsequently, we examined the force prediction error induced by the additional random force in the Langevin thermostat by varying the coupling times to 240 ps, 160 ps, 80 ps, and 40 ps.

Figure 5(b) illustrates the dependence of σ_{total} on the coupling times of the Langevin thermostat, while κ is determined in Fig. 5(c) by fitting the data with Eq. (5). Using the fitted linear parameter, the thermal conductivity of wurtzite GaN was obtained by extrapolating to $\sigma_{\text{total}} = 0$. The uncorrected and corrected thermal conductivity of wurtzite GaN, obtained from NEP-MD simulations along with experimental data, DFT results, and SW-MD simulation results are presented in Fig. 5(d). The calculated thermal conductivities of pure wurtzite GaN from Lindsay *et al.*[5] and Wu *et al.*[12] are significantly higher than experimental values[11] due to differences in lattice constants in wurtzite GaN. The uncorrected thermal conductivities are consistently lower than the other results due to the presence of force prediction errors in the NEP-MD calculations. Interestingly, the corrected thermal conductivity of wurtzite GaN from NEP-MD simulations is 259±6 W/(m·K), which aligns well with the experimental value of 246 W/(m·K). The slight overestimation in our results may be attributed to the weak quantum effect at room temperature. Based on the force error correction method, the intrinsic thermal conductivity of wurtzite GaN along both the x and y directions is calculated to be 272.9 W/(m·K). These values are consistent with those from first-principles calculations: 263 W/(m·K)[7] and 275 W/(m·K)[38] along the in-plane direction. Both the thermal conductivities calculated from NEP and DFT calculations are slightly higher than the experimental value of 234 W/(m·K), which may be ascribed to factors such as threading dislocation density and overall sample quality in the experimental measurement.[11]

Overall, we have achieved an accurate prediction of the pure wurtzite GaN thermal conductivity based on NEP-MD simulations. This work broadens the applicability of the force error correction method to a wider range of materials. Furthermore, our findings confirm that wurtzite GaN does not exhibit significant isotopic effects, in contrast to earlier theoretical works.

4. Conclusions

In conclusion, we successfully developed a neuroevolution potential for wurtzite GaN and accurately predicted its thermal conductivity, achieving excellent agreement with reported experimental measurements. This work effectively addresses the common underestimation issue associated with predicting high thermal conductivity of materials using machine learning potentials. The influence of the hyperparameters of two cutoff radii in NEP models on reproduced energy and force, structural features, computational efficiency, and spectral thermal conductivity was systematically analyzed, and the optimized cutoff radius of 4.5 Å was found to achieve a balance between computational efficiency and accuracy. Furthermore, the force error correction method for NEP models effectively reduces the error arising from the additional force noise in the Langevin thermostat by extrapolating to the zero-force-error limit. This study provides valuable insights and holds significant implications for advancing efficient thermal management technologies in wide-bandgap semiconductor devices.

Acknowledgements

This work was supported by the National Natural Science Foundation of China (Grant Nos. 52376063 and 52306116), the Hebei Key Laboratory of Low Carbon and High Efficiency Power Generation Technology Prevention Fund (Grant No. 2022-K03), and the China Postdoctoral Science Foundation (Grant No. 2023MD744223).

References

[1] Kozak J P, Zhang R, Porter M, Song Q, Liu J, Wang B, Wang R, Saito W and Zhang Y 2023 *IEEE Trans. Power Electron.* **38** 8442
[2] Hoo Teo K, Zhang Y H, Chowdhury N, Rakheja S, Ma R, Xie Q Y, Yagyu E, Yamanaka K, Li K X and Palacios T 2021 *J. Appl. Phys.* **130** 160902
[3] Qin Y, Albano B, Spencer J, Lundh J S, Wang B Y, Buttay C, Tadjer M, DiMarino C and Zhang Y H 2023 *J. Phys. D: Appl. Phys.* **56** 093001
[4] Abdullah M F, Mat Hussin M R, Ismail M A and Wan Sabli S K 2023 *Microelectron. Eng.* **273** 111958
[5] Lindsay L, Broido D A and Reinecke T L 2012 *Phys. Rev. Lett.* **109** 095901
[6] Togo A, Chaput L and Tanaka I 2015 *Phys. Rev. B* **91** 094306
[7] Tang D S, Qin G Z, Hu M and Cao B Y 2020 *J. Appl. Phys.* **127** 035102

[8] Mion C, Muth J F, Preble E A and Hanser D 2006 *Appl. Phys. Lett.* **89** 092123
[9] Simon R B, Anaya J and Kuball M 2014 *Appl. Phys. Lett.* **105** 202105
[10] Rounds R, Sarkar B, Sochacki T, Bockowski M, Imanishi M, Mori Y, Kirste R, Collazo R and Sitar Z 2018 *J. Appl. Phys.* **124** 105106
[11] Zheng Q Y, Li C H, Rai A, Leach J H, Broido D A and Cahill D G 2019 *Phys. Rev. Mater.* **3** 014601
[12] Wu R K, Hu R and Luo X B 2016 *J. Appl. Phys.* **119** 145706
[13] Sun J S, Li S H, Tong Z, Shao C, Chen X C, Liu Q Q, Xiong Y C, An M and Liu X J 2024 *Phys. Rev. B* **109** 134308
[14] Zhou X W, Aubry S, Jones R E, Greenstein A and Schelling P K 2009 *Phys. Rev. B* **79** 115201
[15] Liang Z, Jain A, McGaughey A J H and Keblinski P 2015 *J. Appl. Phys.* **118** 125104
[16] Korotaev P, Novoselov I, Yanilkin A and Shapeev A 2019 *Phys. Rev. B* **100** 144308
[17] Qian X, Peng S, Li X, Wei Y and Yang R 2019 *Mater. Today Phys.* **10** 100140
[18] Fan Z, Zeng Z, Zhang C, Wang Y, Song K, Dong H, Chen Y and Ala-Nissila T 2021 *Phys. Rev. B* **104** 104309
[19] Fan Z Y, Wang Y Z, Ying P H, Song K K, Wang J J, Wang Y, Zeng Z Z, Xu K, Lindgren E, Rahm J M, Gabourie A J, Liu J, Dong H K, Wu J Y, Chen Y, Zhong Z, Sun J, Erhart P, Su Y and Ala-Nissila T 2022 *J. Chem. Phys.* **157** 114801
[20] Bussi G and Parrinello M 2007 *Phys. Rev. E* **75** 056707
[21] Kovács D P, Batatia I, Arany E S and Csányi G 2023 *J. Chem. Phys.* **159** 044118
[22] Hjorth Larsen A, Jørgen Mortensen J, Blomqvist J, *et al.* 2017 *J. Phys.: Condens. Matter* **29** 273002
[23] Kresse G and Furthmüller J 1996 *Phys. Rev. B* **54** 11169
[24] Perdew J P, Burke K and Ernzerhof M 1996 *Phys. Rev. Lett.* **77** 3865
[25] Momma K and Izumi F 2008 *J. Appl. Crystallogr.* **41** 653
[26] Song K K, Zhao R, Liu J H, *et al.* 2024 *Nat. Commun.* **15** 10208
[27] Bernetti M and Bussi G 2020 *J. Chem. Phys.* **153** 114107
[28] Bussi G, Donadio D and Parrinello M 2007 *J. Chem. Phys.* **126** 014101
[29] Fan Z Y, Dong H K, Harju A and Ala-Nissila T 2019 *Phys. Rev. B* **99** 064308
[30] Wang Y, Fan Z, Qian P, Caro M A and Ala-Nissila T 2023 *Phys. Rev. B* **107** 054303
[31] Lv W and Henry A 2016 *New J. Phys.* **18** 013028
[32] Sääskilahti K, Oksanen J, Tulkki J, McGaughey A J H and Volz S 2016 *AIP Adv.* **6** 121904
[33] Fan Z A O, Hirvonen P, Pereira L F C, Ervasti M M, Elder K R, Donadio D A O, Harju A and Ala-Nissila T 2017 *Nano Lett.* **17** 5919
[34] Ying P H and Fan Z Y 2024 *J. Phys.: Condens. Matter* **36** 125901
[35] Ruf T, Serrano J, Cardona M, Pavone P, Pabst M, Krisch M, D'Astuto M, Suski T, Grzegory I and Leszczynski M 2001 *Phys. Rev. Lett.* **86** 906
[36] Zhang H G, Gu X K, Fan Z Y and Bao H 2023 *Phys. Rev. B* **108** 045422
[37] Liang T, Ying P H, Xu K, Ye Z Q, Ling C, Fan Z Y and Xu J B 2023 *Phys. Rev. B* **108** 184203
[38] Xue J, Li F Y, Fan A R, Ma W G and Zhang X 2024 *Int. J. Heat Mass Transfer* **233** 126049
[39] Wu X G, Zhou W J, Dong H K, Ying P H, Wang Y Z, Song B, Fan Z Y and Xiong S Y 2024 *J. Chem. Phys.* **161** 014103
[40] Zhou W J, Liang N J, Wu X G, Xiong S Y, Fan Z Y and Song B 2025 *Mater. Today Phys.* **50** 101638